International Symposium
On Turbulence and Shear Flow
Phenomena (TSFP-8)
August 28 - 30, 2013 Poitiers, France

DIRECT NUMERICAL SIMULATION OF TURBULENT PIPE AT HIGH REYNOLDS NUMBERS, VELOCITY STATISTICS AND LARGE SCALE MOTIONS

Bendiks Jan Boersma
Department of mechanical engineering
Delft University of Technology
Leeghwaterstraat 44, 2628 CA Delft, The Netherlands
email: b.j.boersma@tudelft.nl

ABSTRACT

In recent years there has been a considerable research effort dedicated to turbulent pipe flow. Topics of interest are, amongst others, the scaling of near wall turbulent statistics and the existence of very large scale turbulent structures at higher Reynolds numbers. These structures have been observed experimentally in boundary layers, Hutchins & Marusic (2007) and pipes, Monty *et al.* (2007). Recently these structures have also been observed in moderate Reynolds number direct numerical simulations of channel and boundary layer flows. In this paper we will report on the simulation of turbulent pipe flow at bulk Reynolds numbers of 24600, 37500, and 75,000. The numerical grid (up to 7.6e9 grid nodes) is comparable to the grid used by Jimenez & Hoyas (2008) and should be sufficiently fine to resolve all scales. At high Reynolds numbers we observe some evidence of the aforementioned long scale structures.

Introduction

From an engineering point of view turbulent pipe flow is a very important flow geometry, because of its wide range of technical applications. Although most engineering problems involving pipe flows can be solved by simple engineering correlations, there is still considerable fundamental interest in turbulent pipe flow. One of the open questions is the scaling of turbulent statistics in pipe flows. For instance, in the past it has been argued that the peak of the axial root mean square (rms) value of the turbulent fluctuations is nearly constant and thus independent of the Reynolds number, see for instance Mochizuki & Nieuwstadt (1996). However, the Princeton super pipe experiments indicate that there is a strong dependence of the peak value of the axial rms on the Reynolds number, see for instance McKeon *et al.* (2004). In a recent paper by Hultmark, Bailey & Smits, (2010) a new calibration procedure has been used for the probe which is more accurate for low values of the velocity, hence it should be more reliable near the curved pipe wall. The new calibration gives results which are more or less in line with the observation of Mochizuki & Nieuwstadt (1996).

Large scale meandering structures have been observed in turbulent boundary layers, Hutchins and Marusic (2007), and channel flow Jimenez & Hoyas (2008). They are also experimentally observed in pipe flows, Monty *et al.* (2007). Two point correlations indicate that these structures are considerably longer in pipes than in channels. Hutchins & Marusic (2007) argue that these large scale structures can penetrate into the near wall layer and can make a significant contribution to the kinetic energy in this layer, even down to $D/2-r = 15\nu/u_*$, (where u_* is the friction velocity, D the pipe diameter and ν the kinematic viscosity). This is the location where in general the peak of the turbulent kinetic energy is observed. This statement is consistent with the attached-eddy hypothesis of Townsend (1976). Therefore, it could thus be argued that the long meandering structures could have some influence on the peak value of the axial rms.

Given the points above, and the lack of accurate simulation data for pipe flow, it is in our view useful to perform well resolved direct numerical simulations of pipe flow at high Reynolds numbers. These simulations will be especially useful for the study of near-wall quantities which are very difficult to measure experimentally, especially at high Reynolds numbers where distances to the wall become extremely small.

In contrast to plane channel flow there are for turbulent pipe flow only a limited number of numerical studies carried out, see for instance Eggels *et al.* (1993), Loulou (1997) and Wu & Moin (2008). These models are based on low order finite difference methods and it is expected that the accuracy of the predicted small scales is limited. Therefore, we have developed a new highly accurate numerical model using pseudo spectral techniques in the periodic directions and a 6th order staggered compact finite difference method in the wall normal direction. The algorithm is very similar to the one presented by Boersma (2011) for a duct flow.

Numerical method

The flow in the pipe is governed by the incompressible Navier-Stokes equations. Here we will use the formulation given by White (2008) for a constant viscosity. The equation for conservation of mass in cylindrical coordinates reads:

$$\frac{1}{r}\frac{\partial r u_r}{\partial r}+\frac{1}{r}\frac{\partial u_\theta}{\partial \theta}+\frac{\partial u_z}{\partial x}=0 \qquad (1)$$

where u_r, u_θ, and u_z are the velocity components in the radial, tangential and axial direction respectively. The equa-

tion for conservation of momentum read:

$$\frac{\partial u_r}{\partial t}+\frac{1}{r}\left(\frac{\partial r u_r u_r}{\partial r}+\frac{\partial u_r u_\theta}{\partial \theta}+\frac{\partial r u_r u_z}{\partial z}\right)-\frac{u_\theta^2}{r}=-\frac{1}{\rho}\frac{\partial p}{\partial r}$$
$$+\nu\left(\frac{1}{r}\frac{\partial}{\partial r}\left(r\frac{\partial u_r}{\partial r}\right)+\frac{1}{r^2}\frac{\partial^2 u_r}{\partial \theta^2}+\frac{\partial^2 u_r}{\partial z^2}-\frac{u_r}{r^2}-\frac{2}{r^2}\frac{\partial u_\theta}{\partial \theta}\right)$$

$$\frac{\partial u_\theta}{\partial t}+\frac{1}{r}\left(\frac{\partial r u_r u_\theta}{\partial r}+\frac{\partial u_\theta^2}{\partial \theta}+\frac{\partial r u_z u_\theta}{\partial z}\right)+\frac{u_\theta u_r}{r}=-\frac{1}{\rho r}\frac{\partial p}{\partial \theta}$$
$$+\nu\left(\frac{1}{r}\frac{\partial}{\partial r}\left(r\frac{\partial u_\theta}{\partial r}\right)+\frac{1}{r^2}\frac{\partial^2 u_\theta}{\partial \theta^2}+\frac{\partial^2 u_\theta}{\partial z^2}-\frac{u_\theta}{r^2}+\frac{2}{r^2}\frac{\partial u_r}{\partial \theta}\right)$$

$$\frac{\partial u_z}{\partial t}+\frac{1}{r}\left(\frac{\partial r u_r u_z}{\partial r}+\frac{\partial u_\theta u_z}{\partial \theta}+\frac{\partial r u_z^2}{\partial z}\right)=-\frac{1}{\rho r}\frac{\partial p}{\partial z}+$$
$$\nu\left(\frac{1}{r}\frac{\partial}{\partial r}\left(r\frac{\partial u_z}{\partial r}\right)+\frac{1}{r^2}\frac{\partial^2 u_z}{\partial \theta^2}+\frac{\partial^2 u_z}{\partial z^2}\right)$$

In which u_r, u_θ and u_z are the radial, tangential and axial velocity component, p the pressure, ρ the fluids density, and ν the dynamic viscosity. For stability reasons we have reformulated the non-linear term in the skew symmetric form.

The governing equations are normalized with the friction velocity u_* and the pipe diameter D. The friction velocity is by definition equal to the square root of the wall friction divided by the fluids density, i.e. $u_* = \sqrt{\tau_w/\rho}$. The (frictional) Reynolds number is now defined as $Re_* = u_* D/\nu$ and the bulk Reynolds number $Re_b = (U_b/u_*)Re_*$, where D is the pipe diameter and U_b is the bulk velocity. The distance to the wall $D/2-r$ can be now non-dimensionalised in the following way

$$r^+ = \frac{(D/2-r)u_*}{\nu}$$

Spatial discretization

Most numerical simulation models for pipe flow use 2nd order accurate finite differences. This results in general in a very efficient computational algorithm. However, the accuracy of these 2nd order methods, especially for large wavenumber phenomena is not very good. Therefore, we have chosen in the present study, for a pseudo spectral method combined with a highly accurate 6th order staggered compact finite difference method, which has been developed by us, Boersma (2011)

The Navier-Stokes equations written in cylindrical coordinates are discretized with the pseudo spectral (FFT based) method in the circumferential and axial direction. In the radial direction we use the 6th order staggered compact finite difference method. The grid in the radial direction is nonuniform, with the grid point slightly clustered towards the wall. The compact finite differences itself are computed on a uniform grid with grids pacing ΔR. To be able to use a non-uniform grid in the radial direction a mapping of the following form is used

$$\frac{df}{dr}=\frac{df}{dR}\frac{dR}{dr}$$

where df/dr is the derivative on the non-uniform grid, df/dR the derivative on the uniform grid which will be calculated with the 6th order compact finite difference, and dR/dr maps the non-uniform grid on the uniform grid. Here we use a simple a simple relation for R such that the dR/dr is can be calculated analytically. The derivative df/dR has been calculated with a staggered compact finite difference, see for instance, Boersma (2011)

$$a(f'_{i+1}+f'_{i-1})+f'_i=\frac{b}{\Delta R}(f_{i+1/2}-f_{i-1/2})+ \qquad (2)$$
$$\frac{c}{\Delta R}(f_{i+3/2}-f_{i-3/2}),\ \text{with}\ \ 2\le i\le n-2,$$

In which f'_i is derivative of f with respect to x at point i, ΔR is the (uniform) grid spacing and a, b, and c are yet unspecified coefficients. The coefficients a, b and c can be obtained from a Taylor expansions around grid point i. With the three coefficients a, b, and c in equation (2) we can obtain an 6th order accurate formulation. The values for a, b, and c for this 6th order scheme are:

$$a=9/62,\ b=63/62,\ c=17/186,\ \ 2\le i\le n-2$$

Close to the boundary at points $i=1$ and $i=n-1$ this sixth order formulation can not be used because information from outside the domain would be required. Therefore we use a smaller stencil for these points:

$$a=1/22,\ b=12/11, c=0,\ \ O(\Delta R)^4$$

Which is formally fourth order accurate in ΔR. At the boundary i.e., the points $i=0$ and $i=n$ we use a 3rd or a 4th order accurate formulation:

$$f'_0+23f'_1=\frac{1}{\Delta R}\left(-25f_{1/2}+26f_{3/2}-f_{5/2}\right)+O(\Delta R)^3 \qquad (3)$$

$$f'_0+\frac{331}{15}f'_1=\frac{1}{\Delta R}\left(-\frac{8677}{360}f_{1/2}+\frac{4531}{180}f_{3/2}- \qquad (4)\right.$$
$$\left.\frac{11}{10}f_{5/2}+\frac{1}{36}f_{7/2}+\frac{1}{360}f_{9/2}\right)+O(\Delta R)^4$$

The equation above are for the point $i=0$, for the point $i=n$ similar equations can be derived.

Temporal discretization

The time integration is splitted into two steps. In the first step the velocity is integrated to an intermediate level u^* with help of 3rd order Adams-Bashforth method

$$\mathbf{u}^*-\mathbf{u}^n=\Delta t\left[\frac{23}{12}f(R^n)-\frac{16}{12}f(R^{n-1})+\frac{5}{12}f(R^{n-2})\right]+O(\Delta t)^3 \qquad (5)$$

Where Δt is the time step, $f(R^{n-j})$ denotes all the spatial derivatives in the governing equation at time $t=(n-j)\Delta t$. Subsequently in the pressure correction scheme, the pressure at time level $n+1/2$ is used to calculate the velocity at time level $n+1$:

$$\mathbf{u}^{n+1}=\mathbf{u}^*-\Delta t\frac{1}{\rho}\nabla p^{n+1/2} \qquad (6)$$

So far the pressure at the time level $n+1/2$ is unknown but it can be be computed from a Poisson equation which can be derived by taking the divergence of equation (6), and enforcing the divergence to zero at time level $n+1$

$$\nabla \cdot \mathbf{u}^{n+1} = \nabla \cdot \mathbf{u}^{*} - \frac{\Delta t}{\rho} \nabla \cdot \left(\nabla p^{n+1/2} \right) = 0. \qquad (7)$$

$$\nabla \cdot \mathbf{u}^{*} = \frac{\Delta t}{\rho} \nabla \cdot \left(\nabla p^{n+1/2} \right) \qquad (8)$$

After the solution of the pressure $p^{n+1/2}$ from the Poisson equation, equation (7), the final velocity $\mathbf{u}^{n+1}$ can be computed with help of equation (6). It should be noted that for a consistent formulation it is essential to use the form given by equation (8) and not to replace the left hand side by the Laplacian of the pressure.

Implementation and data storage

The algorithm outlined above is implemented in Fortran 90 using BLAS and LAPACK libraries. The parallization has been done with the 2D pencil library: *2decomp&fft* . This library is build on top of the message passing interface (MPI). The library is freely available from http://www.2decomp.org. The newly developed DNS code scales well up to 24,000 CPU's (it actually scales in the same way as *2decomp&fft* because all communication in the code is handled by this library.

In the following section we will present results of three simulations, with Reynolds numbers of 24,600, 35,000 and 75,000 (based on the bulk velocity and pipe diameter). The corresponding Reynolds numbers based on the friction velocity are 360, 1842 and 3685. In all cases the pipe length is equal to 18 diameters. This length is considerable longer than the length used in the majority of the direct numerical simulations. We expect that we need this length to be able to capture the long structures in the flow. The axial gridspacing is in all simulated cases is less than 10 plus units (less than $10r^{+}$), the maximum circumferential gridspacing is always smaller than 5 plus units and the radial gridspacing near the wall is ≈ 0.5 plus units. For the highest Reynolds number this results in a grid of $440 \times 2400 \times 7200$ gridpoints in the radial, circumferential and axial direction respectively. The simulations are all started on a course grid. The course grid results are interpolate to a finer grid en eventually to grid with the characteristics given before. On this grid the simulations are run sufficiently long to obtain a statistical steady state. Once the simulation have reached this state 100 to 150 full velocity and pressure fields are stored for statistical postprocessing. For the finest grid this gives a data base of approximately 25Tb. All the data sets are stored on a locally available raid system. After the simulation is completed these data sets are post-processed on a serial computer system.

Results

To give an impression of the flow we first present in Figure 1 he instantaneous axial velocity in the $r-\theta$ plane for the three different Reynolds Numbers. With increasing Reynolds number clearly the near wall structures become smaller.

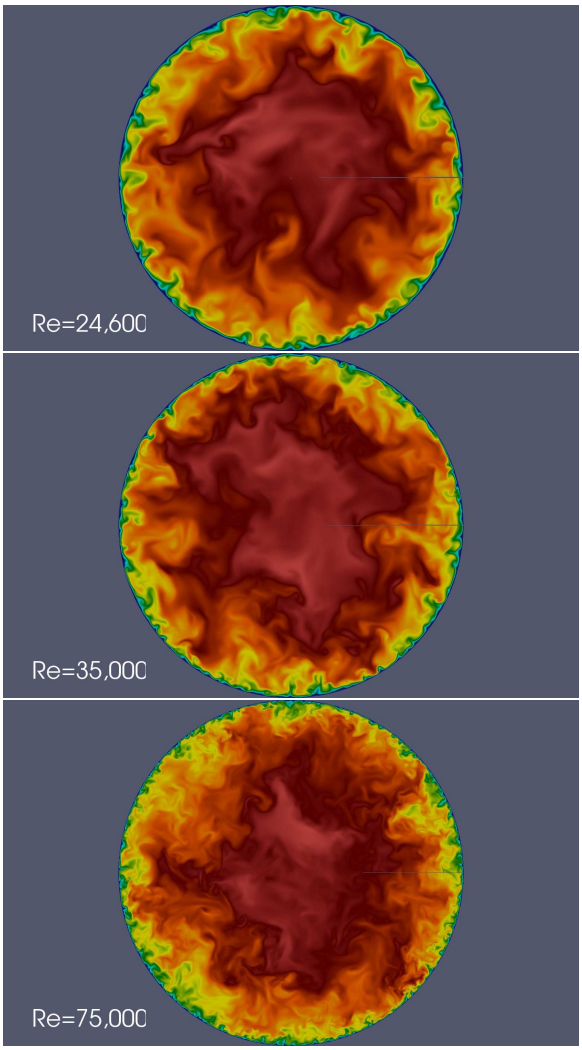

Figure 1. The mean axial velocity for three different Reynolds numbers (24,600, 35,000 and 75,000.

In Figure 2 we show the mean velocity profiles obtained from the three DNS simulations. In Figure 3 we show the wall normal root mean square profiles obtained from the simulations. In this figure we also included the experimental data by Den Toonder & Nieuwstadt (1997) for a Reynolds number of 24,800. Away from the wall the agreement between the experimental data and the simulation is very good. Close to the wall the agreement is less. This is probably due to difficulties in the measurement close to the pipe wall. For increasing Reynolds number the peak value of the radial rms is slightly increasing while the value at the centerline remains constant. In Figure 4, we report the axial root mean square profiles. In this figure we have again included the experimental data of the Den Toonder & Nieuwstadt (1997), showing a very good agreement between simulations and experiment. In Figure 5 we show the Reynolds shear stress and in Figure 6 we show the flatness of the radial velocity (kurtosis). All the profiles presented in Figure 2 to 6 show a slight dependence on the Reynolds number. Furthermore, it is observed that the values of the second (and higher) order statics at the centerline remains constant. In Figure 7 we show the root mean square of the pressure fluctuations. The Reynolds number dependence of the pressure rms is much larger then the Reynolds number dependence of the velocity statistics.

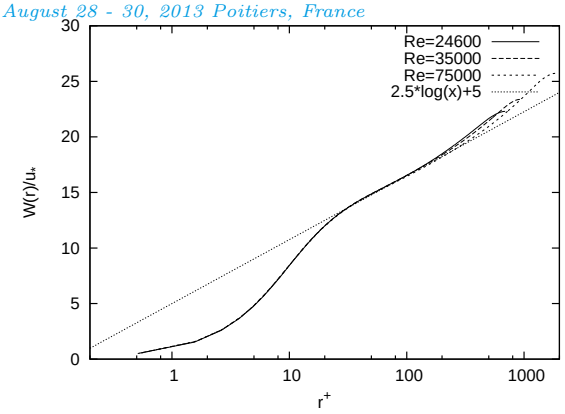

Figure 2. The mean axial velocity as a function of the non-dimensional distance to the wall.

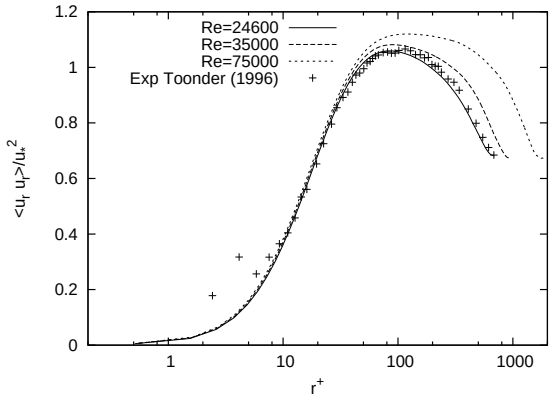

Figure 3. The radial root mean square profiles as a function of the non-dimensional distance to the wall. The symbols denote the experimental data of Den Toonder & Nieuwstadt (1997).

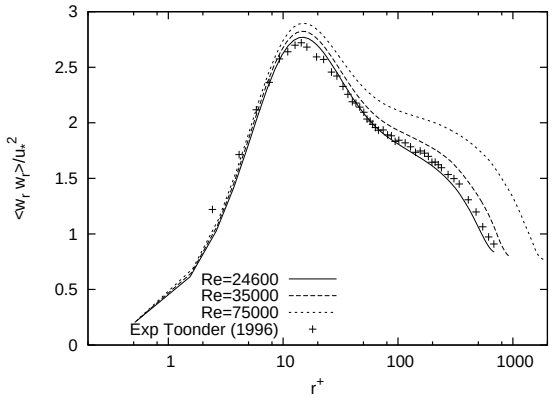

Figure 4. The axial root mean square profiles as a function of the non-dimensional distance to the wall. The symbols denote the experimental data of Den Toonder & Nieuwstadt (1997).

Structures

In Figure 8, we show iso surfaces of the λ_2 criterion. This criterion is to be considered a good measure for vortical structures in the flow. With increasing Reynolds number clearly the size of the vortices decreases and the number greatly increases.

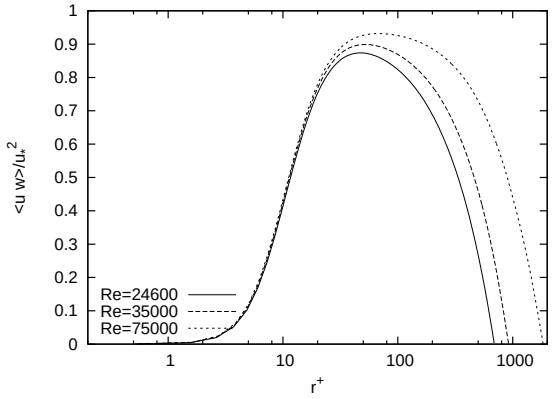

Figure 5. The Reynolds shear stress as a function of the non-dimensional distance to the wall.

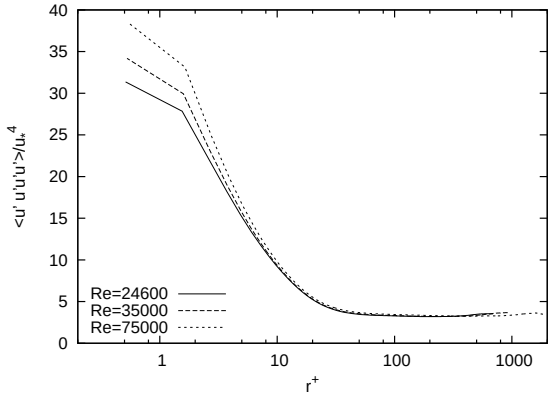

Figure 6. The flatness of the radial velocity (kurtosis) as a function of the non-dimensional distance to the wall.

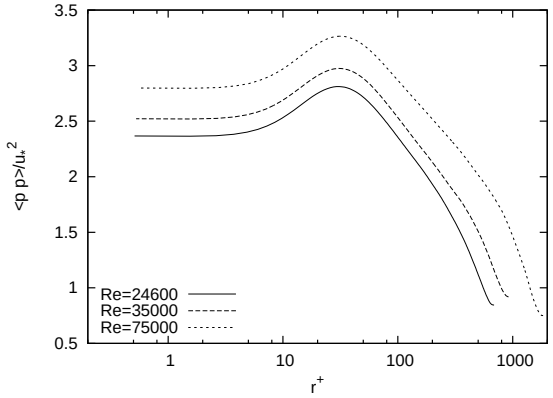

Figure 7. The root mean square of the pressure fluctuations as a function of the non-dimensional distance to the wall.

In Figure 9 we show the instantaneous axial velocity at a cylindrical shell with $r = D/2$ for the low and high Reynolds number case. The spatial extend of the structures is not decreasing with increasing Reynolds number. From 3D visualizations (not shown here) we have the impression that the size of the structures is increasing. This observation is supported by the autocorrelations of the axial velocity presented in Figure 10 for the three different Reynolds numbers. For the highest Reynolds numbers the auto correlations for large z values are somewhat higher than for the

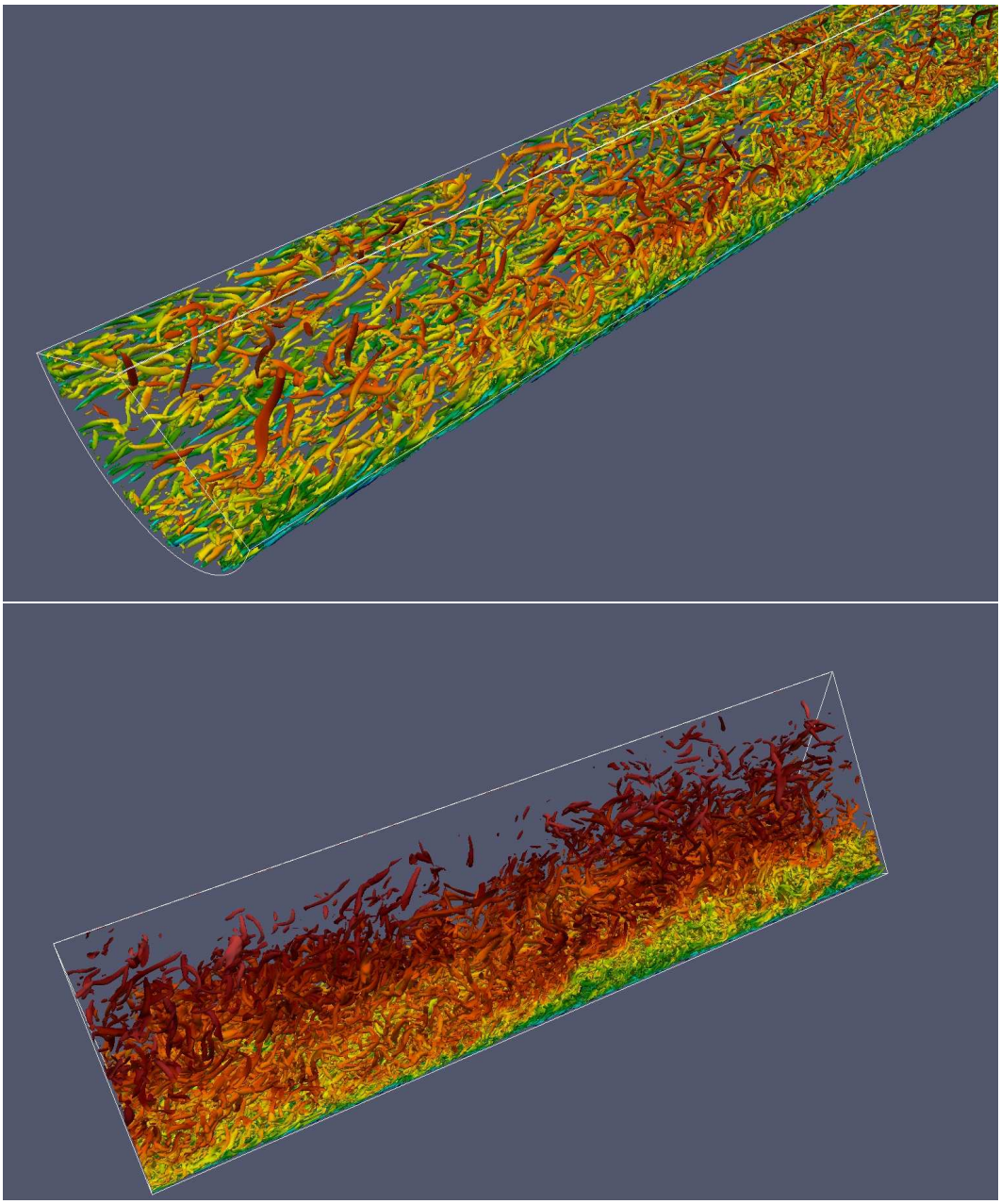

Figure 8. Top: Iso surface of $\lambda_2 = -1e6$ colored with the axial velocity for a Reynolds number of 24,600. bottom the same iso surfaces for a Reynolds number of 75,000. (Due to the large data size especially for the high Reynolds number only a part of the computational domain can be visualized.

lower Reynolds number cases.

Conclusion and future work

In this paper we have present the first results of three well resolved numerical simulations of turbulent pipe flow. The velocity statistics for the low Reynolds number case agree very well with available experimental data. The velocity statistics scaled, with the friction velocity and the non-dimensional distance to the wall show a slight Reynolds number dependence. Visualizations show the existence of large scale motions in high Reynolds number pipe flow. At the moment we have been able to quantitatively this using axial autocorrelation functions. However, the differences in these functions are rather small and better quantification is necessary. This will be explored in the future.

REFERENCES

Boersma, B.J., 2011, A 6th order staggered compact finite difference method for the incompressible Navier-Stokes and scalar transport equations, *J. Comp. Phys.*, **230** 4940-4954.

Den Toonder, J.M.J. & Nieuwstadt, F.T.M., 1997, Reynolds number effects in a turbulent pipe flow for low to moderate Re, *Phys of Fluids*, **9**, 3398.

Jimenez, J. & Hoyas, S., 2008, Turbulent fluctuations above the buffer layer of wall-bounded flows, *J. Fluid Mech.*, **611**, 215-236.

Mochizuki, S., Nieuwstadt, F.T.M., 1996, Reynolds-number-dependence of the maximum in the streamwise velocity fluctuations in wall turbulence, *Exp. in Fluids* , **21**, 218-226.

McKeon, B.J. , Li, J., Jiang, W., Morrison, J.F., & Smits,

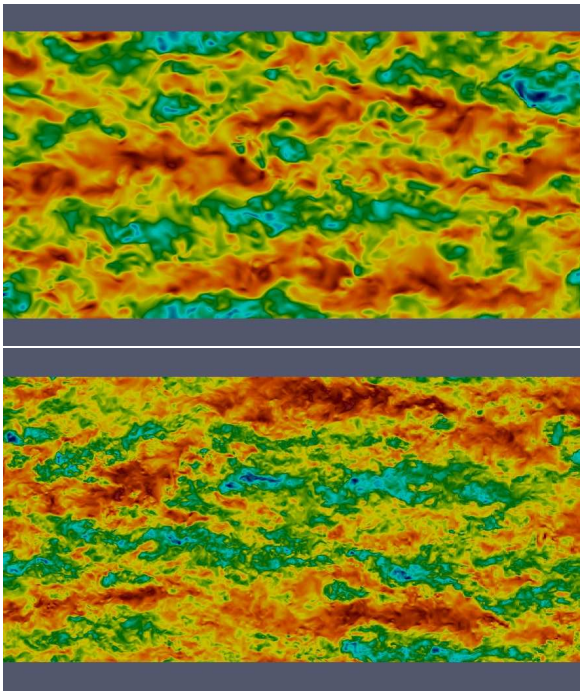

Figure 9. Iso surfaces of the axial velocity at a cylindrical shell with $r = D/2$. The top figure is for a Reynolds number of 24,600 and the bottom figure for a Reynolds number of 75,000.

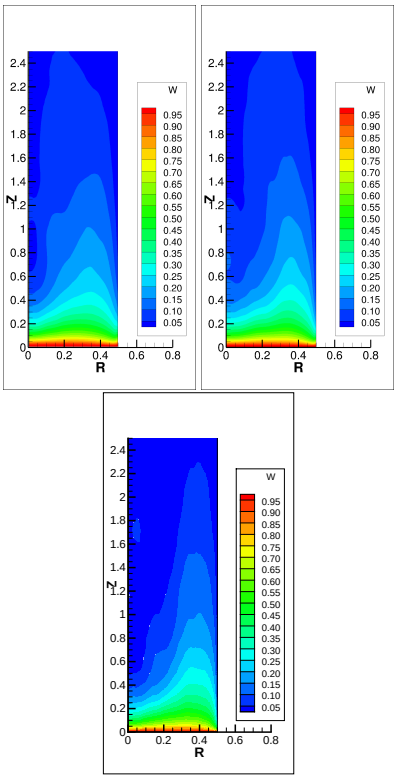

Figure 10. Auto correlations of the axial velocity as a function of the radial distance, for a Reynolds number of 24,600, 35,000 and 75,000.

A.J., 2004, Further observations on the mean velocity distribution in fully developed pipe flow, *J. of Fluid Mech*, **501**, 135-147.

Hultmark, M., Bailey, S.C.C, & Smits, A.J., 2010, Scaling of near-wall turbulence in pipe flow, *J. of Fluid Mech*, **649**, 103-113.

Jimenez, J. & Hoyas, S., 2008, Turbulent fluctuations above the buffer layer of wall-bounded flows, *J. Fluid Mech.*, **611**, 215-236.

Monty, J.P., Stewart, J.A., Williams, R.C., & Chong, M.S., 2007, Large-scale features in turbulent pipe and channel flows, *J. of Fluid Mech.*, **589**, 147-156.

Townsend, A.A., 1976, The structure of turbulent shear flows, Cambridge university press.

White, F.M., 2008, Fluid Mechanics, McGraw-Hill, New York.

Loulou, P., Moser, R.D., Mansour, N., & Cantwell, B., 1997, Direct simulation of incompressible pipe flow using a b-spline spectral method. Technical Report TM 110436, NASA-Ames Res. Center.

Hutchins, N., & Marusic, I., 2007, Evidence of very long meandering features in the logaritmic region of a turbulent boundary layer, *J. of Fluid Mech.* , **579**, 1-28.

Wu, X. & Moin, P., 2008, A direct numerical simulation study on the mean velocity characteristics in turbulent pipe flow, *J. of Fluid Mech.* , **608**, 81-112

Eggels, J.G.M, Unger, F., Weiss, M., Westerweel, J., Adrian, R.J., Friedrich, R., & Nieuwstadt, F.T.M., 1993, Fully developed turbulent pipe flow: a comparison between direct numerical simulation and experiment, *J. of Fluid Mech*, **268**, 175-209.